International Journal of Automation and Computing
www.ijac.net

18(5), October 2021, 681-693
DOI: 10.1007/s11633-021-1308-x

Dynamic System Identification of Underwater Vehicles Using Multi-output Gaussian Processes

Wilmer Ariza Ramirez[1] Juš Kocijan[2,3] Zhi Quan Leong[1] Hung Duc Nguyen[1]
Shantha Gamini Jayasinghe[1]

[1] Australian Maritime College, University of Tasmania, Newnham 7248, Australia

[2] Jožef Steftan Institute, Ljubljana SI-1000, Slovenia

[3] School of Engineering and Management, University of Nova Gorica, Vipara SI-5271, Slovenia

Abstract: Non-parametric system identification with Gaussian processes for underwater vehicles is explored in this research with the purpose of modelling autonomous underwater vehicle (AUV) dynamics with a low amount of data. Multi-output Gaussian processes and their aptitude for modelling the dynamic system of an underactuated AUV without losing the relationships between tied outputs are used. The simulation of a first-principle model of a Remus 100 AUV is employed to capture data for the training and validation of the multi-output Gaussian processes. The metric and required procedure to carry out multi-output Gaussian processes for AUV with 6 degrees of freedom (DoF) is also shown in this paper. Multi-output Gaussian processes compared with the popular technique of recurrent neural network show that multi-output Gaussian processes manage to surpass RNN for non-parametric dynamic system identification in underwater vehicles with highly coupled DoF with the added benefit of providing the measurement of confidence.

Keywords: Dependent Gaussian processes, dynamic system identification, multi-output Gaussian processes, non-parametric identification, autonomous underwater vehicle (AUV).

Citation: W. Ariza Ramirez, J. Kocijan, Z. Q. Leong, H. D. Nguyen, S. G. Jayasinghe. Dynamic system identification of underwater vehicles using multi-output Gaussian processes. *International Journal of Automation and Computing*, vol.18, no.5, pp.681–693, 2021. http://doi.org/10.1007/s11633-021-1308-x

1 Introduction

Dynamic modelling of unmanned underwater vehicles (UUVs) has been a subject of interest among researchers since the early days of underwater exploration. Nowadays, UUVs are extensively employed in research, industry, and military applications. Modelling of autonomous underwater vehicles (AUVs) is an important step for mission design, control and navigation systems. Thus, accurate modelling and adaptability of such systems is an important issue due to such extensive applications. The most common methodologies use a mathematical model which is derived from Newtonian-Lagrange mechanics. This mathematical model is composed of a series of coefficients that need to be calculated to obtain an accurate model. Similarly, a possibility is the use of quaternion formulation for angular position description and the Lagrange method to compute a mathematical model, this option also requires the calculation of model coefficients but reduces the use of trigonometric functions[1]. The difference between the obtained model and the reality is usually treated in the literature as noise and, in most cases, is modelled as a Gaussian distribution. A Gaussian distribution can be extended to the calculation of an approximation to a real model of a vehicle with higher exactitude and adaptability than a mathematical model[2].

Over the years, multiple methods for the calculation of coefficients of underwater vehicles have been proposed. One way to obtain the hydrodynamic coefficients is to perform a series of captive model tests such as rotating arm and planar motion mechanics[3–5]. Allotta et al.[6] proposed a method with field test and using onboard telemetry to develop a simplified model of underwater vehicles, despite the excellent results, the resultant model can only be applied to specific tasks as it lags the rigor required for high precision control task as path following. The most elaborated techniques presented by [7] include modelling the effects produced by the propulsion to the model coefficients. These techniques require even a larger set of experiments. Another common technique for the hydrodynamic coefficient calculation is the use of computational fluid dynamics (CFD)[8]. However, for the suc-

Research Article
Manuscript received February 28, 2021; accepted June 8, 2021; published online July 13, 2021
Recommended by Associate Editor Min Wu
Colored figures are available in the online version at https://link.springer.com/journal/11633

cessful application, CFD still requires verification of results with experiments[9].

Nevertheless, research has probed the variability of mathematical models for AUVs as the vehicle operates in proximity to objects[10, 11], near-surface[12], and most commercially available underwater vehicles with a modular architecture involving variable geometric and mass[13]. Furthermore, in certain applications, the precision of some coefficients is required to be within 5% of accuracy[14]. Therefore, the variability of coefficients and the high precision required to make it cumbersome or even impossible to acquire a single exact analytical system model based on physical rules.

Another procedure to obtain coefficients from a model of an underwater vehicle is the use of observers. Common observers applied to obtain the hydrodynamic coefficients of AUVs from measured data are least-squares[15, 16], nonlinear Kalman filters such as extended (EKF), and unscented Kalman filter (UKF)[17]. The EKF requires the linearization at each time step to approximate non-linearities, which can be difficult to regulate and implement. A method to overcome this is the use of UKF, which applies the unscented transform over a set of methodically chosen samples to model the system′s nonlinearity[18, 19] employed the extended Kalman particle filter (EKPF) to improve the estimation of coefficients for underwater vehicles for navigation. Other common methodologies are frequency domain identification[20], neural networks (NN)[21] and support vector machines (SVM)[22]. The latter two methodologies are machine learning algorithms and are more commonly used in online learning of the coefficients and provide system adaptability. The adaptation of the mathematical model has inherent defects such as the dependency of initial values, small quantity of coefficients to be updated, ill-conditioned matrix, and drift. The variability of the calculated model can be exacerbated if it is considered that modern vehicles are modular and new modules with different properties are added or removed from the vehicle in dependence mission goals[23].

Machine learning algorithms are not limited to the calculation of hydrodynamic coefficients as they can learn to behave as part of the system or the complete system. Multiple applications have taken advantage of this ability and used NN[24] and SVM[25] to learn the damping model for the system, which is placed in parallel to a well-known partial mathematical model. Other applications have used pure machine learning algorithms to identify a complete underwater vehicle as a black-box model with the use of a nonlinear autoregressive model with exogenous (NARX) architecture. Kodogiannis et al.[26] have used multiple architectures of NN for the regression of an AUV model in a NARX architecture and used the learned model for model predictive control. Their study shows that recurrent NN (RNN) provides higher faithfulness to the plant. It can be considered that most of these applications are parametric machine learning algorithms as the algorithm has a fixed number of parameters. This characteristic allow faster computation, but makes stronger assumptions about the data and may perform badly if the assumptions are wrong[27].

Another option is the employment of non-parametric machine learning algorithms. A non-parametric algorithm assumes that the data distribution cannot be defined in terms of a finite set of parameters. The number of parameters grows as it learns from more data. An example of non-parametric machine learning algorithm is GP[27]. Non-parametric GPs applied to an underwater vehicle can improve techniques that employ vehicle models as control[28] and navigation[29]. In geostatistics, GP is a well-established methodology, where the method is called "kriging"[30]. In GPs-based system identification, the model is learned over input-output data, and a covariance function is employed to represent the vehicle behaviour. GPs are better suited to work with noisy data and small quantities of data. The predicted results of a GP consist of a mean and variance value that can be exploited for other purposes, such as navigation, control, and model-based fault detection. It contains a measure of confidence.

Recently, Wehbe et al.[31] compared different machine learning algorithms for the system regression of underwater vehicles, i.e., NN, SVM, Gaussian process regression (GPR), and Kernel ridge regression (KRR). Their results show that the machine learning algorithms could model an AUV from onboard sensor data compared to a least-squares approach. Nevertheless, in their study, a structure for dynamic system identification has not been employed, and each degree of freedom was treated as a separate element. This can be problematic in AUVs as the outputs are strongly coupled. In the specific case of modelling with GPs[2], research shows that the dynamic regression of a system with GPs can produce better results than other methodologies. The most common methodology for multi-input-multi-output systems is to model each DoF as a separate system[32]. Ariza Ramirez et al.[33] used GPs modelling for the application of model-based reinforced learning to control underwater vehicles. In this research, a single GPs model was employed for each DoF, and the coupling between outputs was ignored. The result showed a rapid convergence from on board sensors. More advanced methodologies for dynamic system identification have been proposed in [34, 35]. Specific methodologies are introduced to identify multi-output GPs based on the use of variation of dependent GPs.

Multi-output GP is one of the options for modelling multi-output systems. Multi-output GPs have ability to model the nonlinear behaviour and relation between outputs of a multi-output system[36]. Both characteristics are important for AUV dynamics. In this study, a non-parametric dynamic system identification with multi-output GPs architecture employed by the authors, for ships[37] is extended to AUVs. However, the dynamics of ships and

AUV share some similarities; AUVs have more degrees of freedom, higher coupling between outputs, and higher nonlinearities. The differences between ships and AUV force a different required architecture. The output from the algorithm will be a predictive value and a measure of confidence of the predictive value. The objective of the study is the demonstration of the viability and robustness of multi-output GPs in modelling AUVs. Multi-output GPS can allow a new form of controllers and observers that can drastically improve navigation and control of underwater vehicles. The current implementation was made over data obtained from a non-conventional test with a variable frequency of a nonlinear simulation model of a Remus 100 AUV. Multiple sample times and data length were tested to find the best metric that can describe an AUV. RNN was employed as a comparison to measure the effectiveness of the proposed method.

2 Nonlinear dynamic AUV model

The nonlinear dynamic equations of motion of an underwater vehicle can be expressed as in [38]. A vector defined by a state vector composed by the vector v of velocities on the body frame of the form $[u, v, w, p, q, r]^{\mathrm{T}}$ and the vector η of position in the Earth fixed frame (Fig. 1) of the form $[\xi, \eta, \zeta, \phi, \theta, \psi]^{\mathrm{T}}$ such that:

$$\boldsymbol{M}\dot{\boldsymbol{v}} + \boldsymbol{C}(\boldsymbol{v})\boldsymbol{v} + \boldsymbol{D}(\boldsymbol{v})\boldsymbol{v} + \boldsymbol{g}(\eta) = \tau \tag{1}$$

with the kinematic equation

$$\dot{\eta} = \boldsymbol{J}(\eta)\boldsymbol{v} \tag{2}$$

where

η is the position and orientation of the vehicle in Earth-fixed frame;

$\boldsymbol{v}$ is the linear and angular vehicle velocity in the body-fixed frame;

$\dot{\boldsymbol{v}}$ is the linear and angular vehicle acceleration in the body-fixed frame;

$\boldsymbol{M}$ is the matrix of inertial terms;

$\boldsymbol{C}(\boldsymbol{v})$ is the matrix of Coriolis and centripetal terms;

$\boldsymbol{D}(\boldsymbol{v})$ is the matrix consisting of damping or drag terms;

$\boldsymbol{g}(\eta)$ is the vector of restoring forces and moments due to gravity and buoyancy;

τ is the vector of control and external forces;

$\boldsymbol{J}(\eta)$ is the rotation matrix that converts velocity from body-fixed frame v to an Earth fixed frame velocity $\dot{\eta}$.

Equation (1) can be expanded into a more general equation of motion as has been shown in [39] and applied in [40]. The result of the expansion will be a system of six equations with 73 hydrodynamic coefficients. However, the expansion of (1) does not include a model for the control surfaces (thrusters and fins). In a general case, Fossen[38] demonstrated that the resulting forces and moments of a control surface can be expressed as

$$\begin{aligned} F_{prop} &= -K_{fprop}\,|n|\,n \\ M_{prop} &= -K_{mprop}\,|n|\,n \end{aligned} \tag{3}$$

$$\begin{aligned} L_{fin} &= K_{L|\delta_{fin}}\delta_{fin}v_e^2 \\ M_{fin} &= K_{M|\delta_{fin}}\delta_{fin}v_e^2. \end{aligned} \tag{4}$$

A more accurate thruster model can be found in [41] with the inclusion of the motor model and fluid dynamics. However, in this study, a more conservative model is used. Details of the Remus 100 AUV model used in this study are given in Section 3.

3 Dynamic identification with multi-output GPs

GPs can be defined as a generalization of a multivariate Gaussian distribution. A multivariate Gaussian distribution is defined by its mean and a covariance matrix. In the case of GPs, they are a distribution over functions rather than a distribution over vectors. GPs is one of the methods based on kernel functions where the kernel function calculates the relationship between an input and an output point, and generates the covariance between them. The covariance determines how strongly linked (correlated) these two points are. In the case of multi-output GPs, this is extended by the convolution of kernels to add not only the relationship between an input and an output but also the relationship between the outputs.

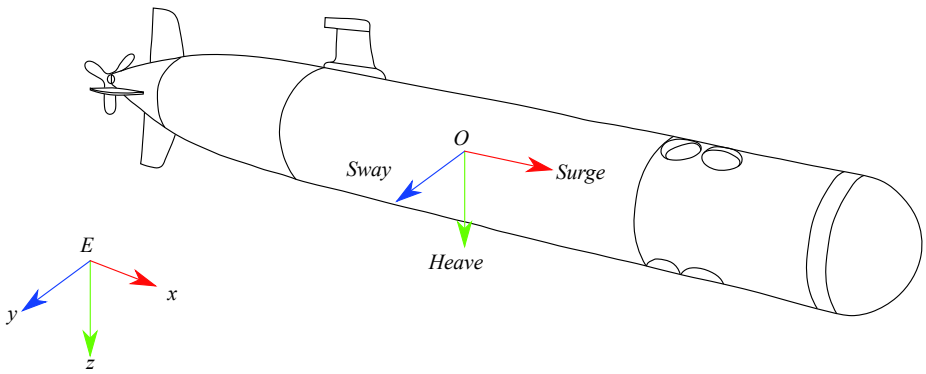

Fig. 1 AUV different reference frames, vehicle frame is equal to centre of buoyancy.

The kernel is the key ingredient for the calculation of the covariance matrix that correlates inputs and outputs of training data[42].

The presented application of multi-output system identification with GPs is based on the previous work by Alvarez and Lawrence[36] that based on their work[2]. Dynamic identification is defined as the search for the relationship between a vector formed by delayed samples from the inputs commands $\boldsymbol{u}(k-1)$, the last system state $\boldsymbol{y}(k-1)$, and the future output values. The relationship can be expressed as

$$\boldsymbol{y}(k+1) = f\left(\boldsymbol{x}(k), \Theta\right) + \boldsymbol{v}(k) \tag{5}$$

where $f\left(\boldsymbol{x}(k), \Theta\right)$ is a function that maps the sample data vector $\boldsymbol{x}(k)$ to the output space based on the hyperparameters Θ; $\boldsymbol{v}(k)$ accounts for the error and noise in the prediction of $\boldsymbol{y}(k)$. In dynamic system identification, the discrete-time variable k is presented as an embedded element in the regression process as it is accounted for in the delayed samples. In this application, the vector $\boldsymbol{x}(k)$ is composed of the vector of regressors and the vector of commanded inputs.

Dynamic system identification of nonlinear systems requires the selection of a nonlinear model structure such as nonlinear autoregressive model with exogenous input (NARX), nonlinear autoregressive (NAR), nonlinear output-error (NOE), nonlinear finite-impulse response (NFIR), and other structures. NARX is the simpler and most popular structure to implement as it only requires measurements of system output(s) and input(s). The difficulties of measuring AUV states makes NARX the most practical structure since the data required can be obtained by the on-board sensors[2].

3.1 Multi-output GPs

Equation (1) shows the level of connection between the Newton-Lagrange equations that define the dynamic system of an AUV. Nonlinearities and integration between outputs can be better represented by multi-output GPs[36]. Multi-output GPs are founded in the regression of data using the convolution of a smoothing kernel function with white noise process[43]. Boyle and Frean[44] introduced the concept machine learning by assuming multiple latent processes defined over a space $\mathbf{R}^q$. The coupling between two related outputs is a model with a common latent process and their independence with a latent function, which does not interact between outputs. If a set of functions $\{f_q\left(\boldsymbol{x}\right)\}_{q=1}^{Q}$ is considered, where Q is the output dimension for an N number of data points, where each function is expressed as the convolution between a latent function $u(\boldsymbol{z})$ and a smoothing kernel $\{k_q\left(\boldsymbol{x}\right)\}_{q=1}^{Q}$, the function can be expressed as

$$f_q(\boldsymbol{x}) = \int_{-\infty}^{\infty} k_q\left(\boldsymbol{x}-\boldsymbol{z}\right) u\left(\boldsymbol{z}\right) \mathrm{d}\boldsymbol{z} \tag{6}$$

Equation (6) can be generalized for more than one latent function $\{u_r\left(\boldsymbol{x}\right)\}_{r=1}^{R}$ and a corruption function (noise) $w_q(\boldsymbol{x})$ independent to each of the outputs can be included,

$$\begin{aligned} \boldsymbol{y}_q\left(x\right) &= f_q\left(\boldsymbol{x}\right) + w_q\left(\boldsymbol{x}\right) \\ \boldsymbol{y}_q\left(x\right) &= \sum_{r=1}^{R} \int_{-\infty}^{\infty} k_{qr}\left(\boldsymbol{x}-\boldsymbol{z}\right) u_r\left(\boldsymbol{z}\right) \mathrm{d}\boldsymbol{z} + w_q\left(\boldsymbol{x}\right). \end{aligned} \tag{7}$$

The covariance between two different functions $\boldsymbol{y}_q\left(\boldsymbol{x}\right)$ and $y_s(\boldsymbol{x}')$ is

$$\begin{aligned} \operatorname{cov}\left[\boldsymbol{y}_q\left(\boldsymbol{x}\right), \boldsymbol{y}_s(\boldsymbol{x}')\right] =& \operatorname{cov}\left[f_q\left(\boldsymbol{x}\right), f_s(\boldsymbol{x}')\right] + \\ & \operatorname{cov}\left[w_q\left(\boldsymbol{x}\right), w_s(\boldsymbol{x}')\right] \delta_{qs} \end{aligned} \tag{8}$$

where

$$\begin{aligned} \operatorname{cov}\left[f_q\left(\boldsymbol{x}\right), f_s(\boldsymbol{x}')\right] = \sum_{r=1}^{R}\sum_{p=1}^{R} \int_{-\infty}^{\infty} k_{qr}(\boldsymbol{x}-\boldsymbol{z}) \times \\ \int_{-\infty}^{\infty} k_{sp}(\boldsymbol{x}'-\boldsymbol{z}') \operatorname{cov}\left[u_r\left(\boldsymbol{z}\right), u_p(\boldsymbol{z}')\right] \mathrm{d}\boldsymbol{z}' \mathrm{d}\boldsymbol{z}. \end{aligned} \tag{9}$$

If it is assumed that $u_r\left(\boldsymbol{z}\right)$ is an independent white noise, $\operatorname{cov}\left[u_r\left(\boldsymbol{z}\right), u_p(\boldsymbol{z}')\right] = \sigma_{ur}^2 \delta_{rp} \delta_{\boldsymbol{z},\boldsymbol{z}'}$ will become:

$$\operatorname{cov}\left[f_q\left(\boldsymbol{x}\right), f_s(\boldsymbol{x}')\right] = \sum_{r=1}^{R} \sigma_{ur}^2 \int_{-\infty}^{\infty} k_{qr}(\boldsymbol{x}-\boldsymbol{z}) k_{sp}(\boldsymbol{x}'-\boldsymbol{z}') \mathrm{d}\boldsymbol{z}. \tag{10}$$

The mean $\widehat{\boldsymbol{y}}'$ with variance $\sigma_{\widehat{\boldsymbol{y}}'}$ of a predictive distribution at the point $\boldsymbol{x}'$ given the hyperparameters $\boldsymbol{\Theta}$ can be defined as

$$\widehat{\boldsymbol{y}}' = \boldsymbol{k}(\boldsymbol{x}', \boldsymbol{x}) \boldsymbol{k}(\boldsymbol{x}, \boldsymbol{x})^{-1} \boldsymbol{y} \tag{11}$$

and variance

$$\sigma_{\widehat{\boldsymbol{y}}'}^{2} = \boldsymbol{k}(\boldsymbol{x}', \boldsymbol{x}') - \boldsymbol{k}(\boldsymbol{x}', \boldsymbol{x})^{\mathrm{T}} \boldsymbol{k}(\boldsymbol{x}, \boldsymbol{x})^{-1} \boldsymbol{k}(\boldsymbol{x}', \boldsymbol{x}). \tag{12}$$

A comprehensive description and implementation of the convolution process can be found in [36] and [45], respectively. In this study, the convolution of two square exponential kernels is used since the squared exponential kernel is a universal kernel[46], provided that data is stationary and the function to be modelled is a smooth one. Furthermore, squared exponential kernel has a small number of hyperparameters to be established.

3.2 Learning hyperparameters

The main methods for learning the hyperparameters Θ of a GP are Bayesian model interference and marginal likelihood. Bayesian inference is based on the concept that prior data of the unknown function to be mapped

are known, and a posterior distribution over the function is refined by the addition of observations. The marginal likelihood takes advantage that some hyperparameters are going to be more recognizable. Based on this, a unimodal narrow Gaussian distribution can describe the hyperparameters posterior distribution.

The learning of GPs hyperparameters Θ is usually done with the maximization of the marginal likelihood. The marginal likelihood can be expressed as

$$p(\boldsymbol{y}|\boldsymbol{x},\boldsymbol{\Theta}) = \frac{1}{(2\pi)^{\frac{N}{2}}|\boldsymbol{K}|^{\frac{1}{2}}} \mathrm{e}^{-\frac{1}{2}\boldsymbol{y}^{\mathrm{T}}\boldsymbol{K}^{-1}\boldsymbol{y}} \tag{13}$$

where N is the number of input learning data points, $\boldsymbol{K}$ is the covariance matrix, and $\boldsymbol{y}$ is a vector of learning output data of the form $[y_1; y_2; \cdots; y_N]$. In order to minimize the calculation complexity, the application of the logarithmical marginal likelihood is preferred. For (13), if logarithmic properties are applied, it can be obtained:

$$\mathcal{L}(\boldsymbol{\Theta}) = -\frac{1}{2}\log(|\boldsymbol{K}|) - \frac{1}{2}\boldsymbol{y}^{\mathrm{T}}\boldsymbol{K}^{-1}\boldsymbol{y} - \frac{N}{2}\log(2\pi). \tag{14}$$

The maximization of log-likelihood, can be done with multiple methods such as genetic algorithms, particle swarm optimization, or gradient descent. The computation of likelihood partial derivatives with respect to each hyperparameter is required for deterministic optimization methods. The log-likelihood derivatives for each hyperparameter can be calculated by [47]:

$$\frac{\partial\mathcal{L}(\boldsymbol{\Theta})}{\partial\boldsymbol{\Theta}_i} = -\frac{1}{2}\mathrm{tr}\left(\boldsymbol{K}^{-1}\frac{\partial\boldsymbol{K}}{\partial\boldsymbol{\Theta}_i}\right) + \frac{1}{2}\boldsymbol{y}^{\mathrm{T}}\boldsymbol{K}^{-1}\frac{\partial\boldsymbol{K}}{\partial\boldsymbol{\Theta}_i}\boldsymbol{K}^{-1}. \tag{15}$$

Equation (14) gives the computational complexity for the learning process, for each cycle, the inverse of the covariance matrix of K must be calculated. The calculation has a complexity $O(NM)^3$. After learning, the prediction complexity is $O(NM)$ and to predict the mean value $\sigma(k+1)$ is $O(NM)^2$ for a value $\boldsymbol{y}(k+1)$. The higher-order term $O(NM)^3$ is the major disadvantage of using multi-output GPs. The complexity of learning the hyperparameters increases in a cubic form with the increase in data points. For larger data sets, methods that do not require partial derivatives such as genetic algorithms, differential equations, and particle swarm optimization can be applied to avoid a high computational cost by reducing the number of total iterations need.

4 Experiment setup and results

4.1 Experiment setup

The implementation of a mathematical model of an underactuated Remus 100 AUV was used to generate the required identification data. The coefficients of [40] were used and adapted for simulation on Simulink. As the original mathematical model produced by [40] has a constant thrust force, the thruster model from [48] that is based on [38] was added. The resultant model was tested to mimic the original results obtained by Prestero[40] at a speed of 1.5 m/s. The AUV details can be found in Table 1. As shown in Fig. 2, a simulation setup was developed in Matlab/Simulink to emulate the AUV behaviour. Fig. 3 shows an example of input signals given for the rudder angle, thruster revolution per minute (RPMs), and elevator angle, respectively. A total of 8 sets of data were produced by combining an initial chirp signal, and after the first 1 000 seconds, the command signal change

Table 1 Remus 100 general characteristics

Parameter	Value
Weight	299 (N)
Buoyancy	306 (N)
Vehicle total length	1.33 (m)
Diameter	0.191 (m)
Max. Depth	100 (m)

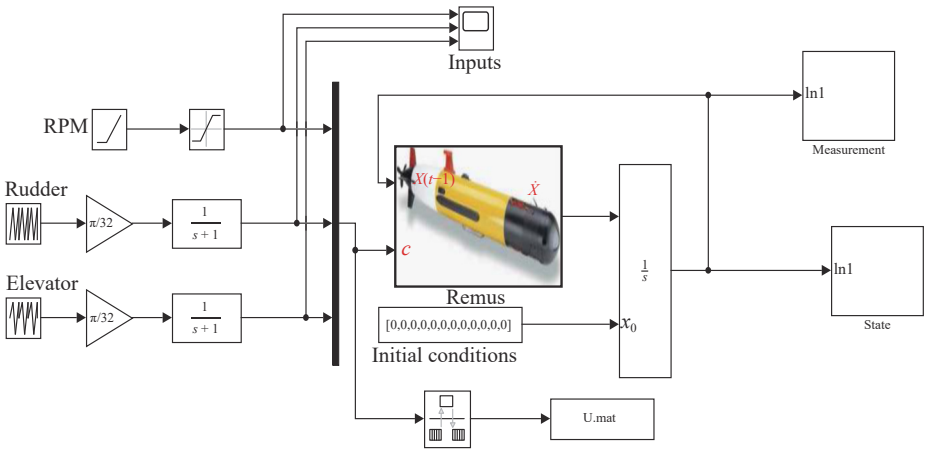

Fig. 2 Remus 100 AUV simulink model

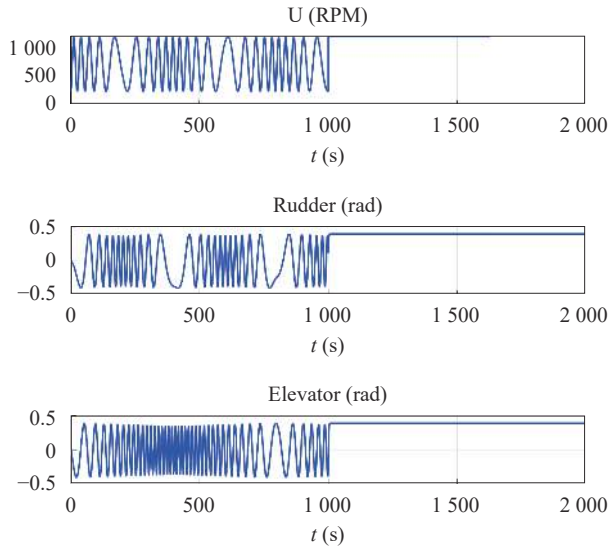

Fig. 3 Remus 100 input signals example chirp + step for all inputs

to a step function or ramp function. The simulation was carried out for 2 000 seconds. A list of simulation done can be seen in Table 2. Standard test, such as the zigzag test or turning circle test were not used as GPs require rich data or large quantities of data. A sample data point was captured for every 1.5 seconds over the input and outputs. A total of 8 000 points were captured over the six motion outputs and 4 000 points over the three input signals (Propeller RPM, rudder angle, and elevator angle). The data set was divided into two sets of points. The first set of points is used for the model learning, this training data is equivalent to the section of the chirp input signal, and the second set of points is used for learning validation. The validation data is chosen to be outside of the training domain and very different fro the training data to test the ability of the method to predict beyond the training range.

4.2 Training and validation

A script was written to implement the NARX structure with multi-output GPs, and the implementation of multi-out GPs by [45] was employed. The multi-output GPs regressors were defined as

$$\begin{bmatrix} \boldsymbol{u}_k \\ \boldsymbol{v}_k \\ \boldsymbol{w}_k \\ \boldsymbol{p}_k \\ \boldsymbol{q}_k \\ \boldsymbol{r}_k \end{bmatrix} = f\left(\boldsymbol{y}, \boldsymbol{c}_{k-1:3}\right) \tag{16}$$

where $\boldsymbol{y}$ is the vector of regressors $[\boldsymbol{u}_{k-1:3}, \boldsymbol{v}_{k-1:3}, \boldsymbol{w}_{k-1:3}, \boldsymbol{p}_{k-1:3}, \boldsymbol{q}_{k-1:3}, \boldsymbol{r}_{k-1:3}]^{\mathrm{T}}$, the function f is a relation between the vector of regressors from the correspondent vehicle speeds $(\boldsymbol{u}, \boldsymbol{v}, \boldsymbol{w}, \boldsymbol{p}, \boldsymbol{q}, \boldsymbol{r})$ or the full vehicle state $\boldsymbol{y}$, and the vector $\boldsymbol{c}$ that content the regressors of the commanded signals to the respective output of the system. The input signals were normalized between −1 and 1 to give all the inputs and outputs the same weight in the learning process. This normalization is required to reduce the possibility of the minimization algorithm being bias to one of the regressors.

For the training, a minimum search with the gradient descent method, particularly the interior-point algorithm, was used to minimize the negative logarithmical likelihood.

Two nonlinear system identification models with neural networks were also implemented for comparison. The NN systems are recurrent neural networks (RNN), as shown in Figs. 4 and 5. The first MIMO RNN (RNN 1, Fig. 4) was setup with three terms of delays for the output to be feedback to the network and three terms delay of the inputs. The RNN 1 that was selected as relatively optimal for the task at hand used two hidden layers with logarithmic sigmoid functions for the hidden layer neurons and was trained with Levenberg-Marquardt back-

Table 2 Simulation description

Experiment number	Experiment configuration
1	Chirp+ramp in propeller
2	Chirp+ramp in rudder
3	Chirp+ramp in stern
4	Chirp+ramp in all surfaces
5	Chirp+step in propeller
6	Chirp+step in rudder
7	Chirp+step in stern
8	Chirp+step in all surfaces

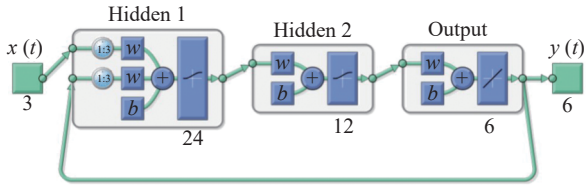

Fig. 4 RNN 1 configuration for AUV identification

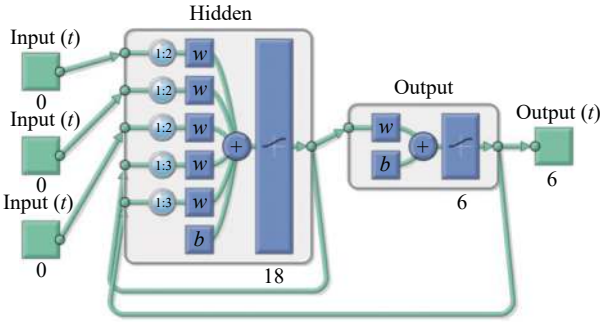

Fig. 5 RNN 2 configuration for AUV identification

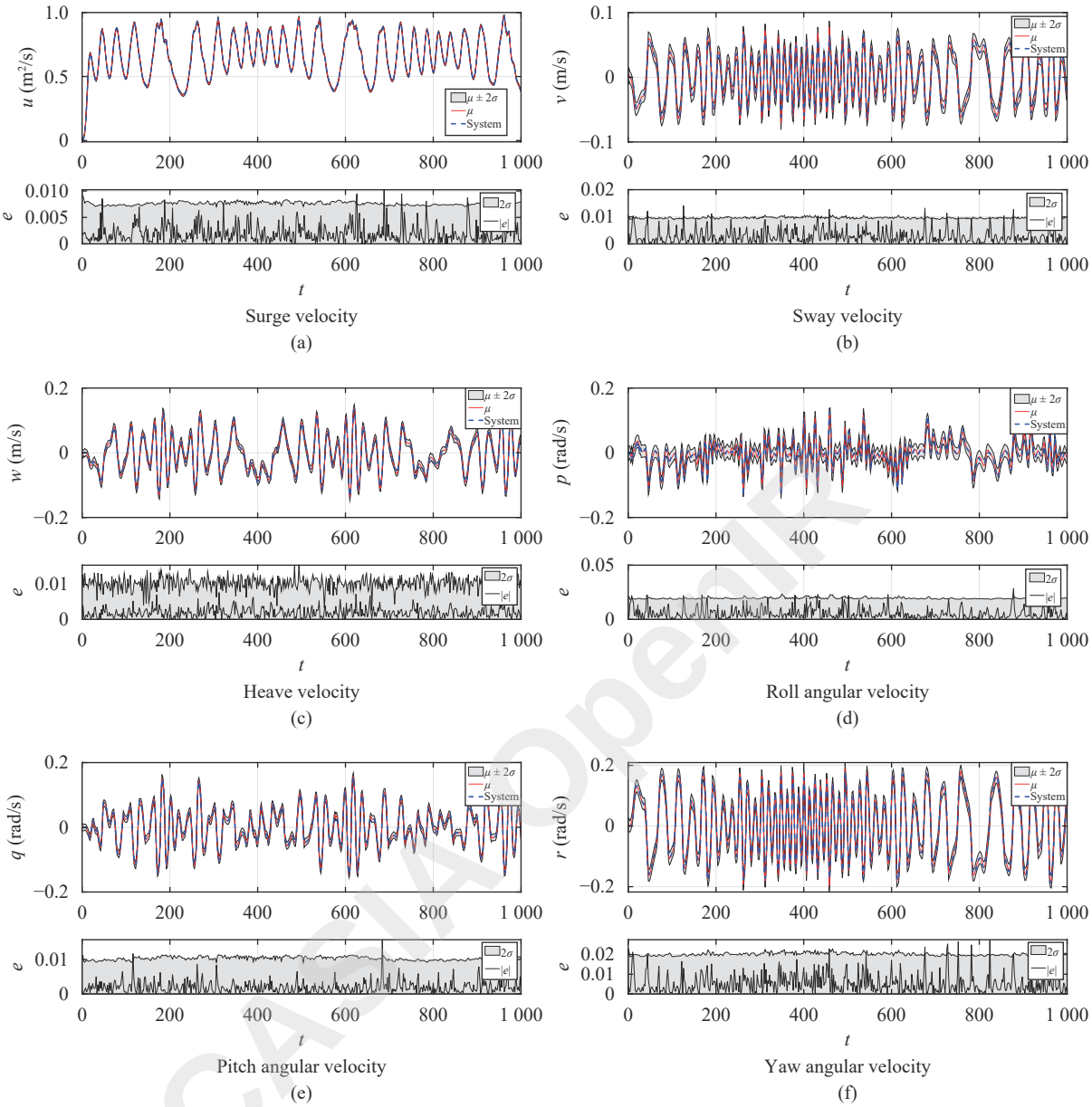

Fig. 6 Multi-output GPs training velocity plots

propagation. This configuration and regressors were selected as they provide the best results for our system. RNN 2 (Fig. 5) is a fully connected RNN with a single hidden layer. RNN 2 use the same logarithmic sigmoid functions for the hidden layer of neurons and was trained with Levenberg-Marquardt backpropagation. The third step of simulation was carried out with the combination of the full length of the data and feeding back after each step the delayed output from the model. The neural network system was trained, validated, and tested with the same data used for the multi-output GPs. The complete implementation code can be found at the GitHub Repository[1]. Fig. 6 presents the prediction results of GPs training compared to the ground truth from the AUV simulator and the error plots between the predicted and real systems. In Figs. 6–8, a 2σ variance is plotted. The variance values of the training data are in the expected value and encompass the error results.

The validation data consisted of the second part of the captured data in vector form and the real output from the training data with the respective system delays. The segments of the results from the validation with the second set of data are depicted in Fig. 7. The low validation errors show a good system prediction for all degrees of freedom.

4.3 Simulation

With the objective to test the ability of the learning system, a simulation stage was implemented for the

[1]https://github.com/ArizaWilmerUTAS/System-indetification-of-underwater-vehicles-with-Multi-Output-Gaussian-Processes

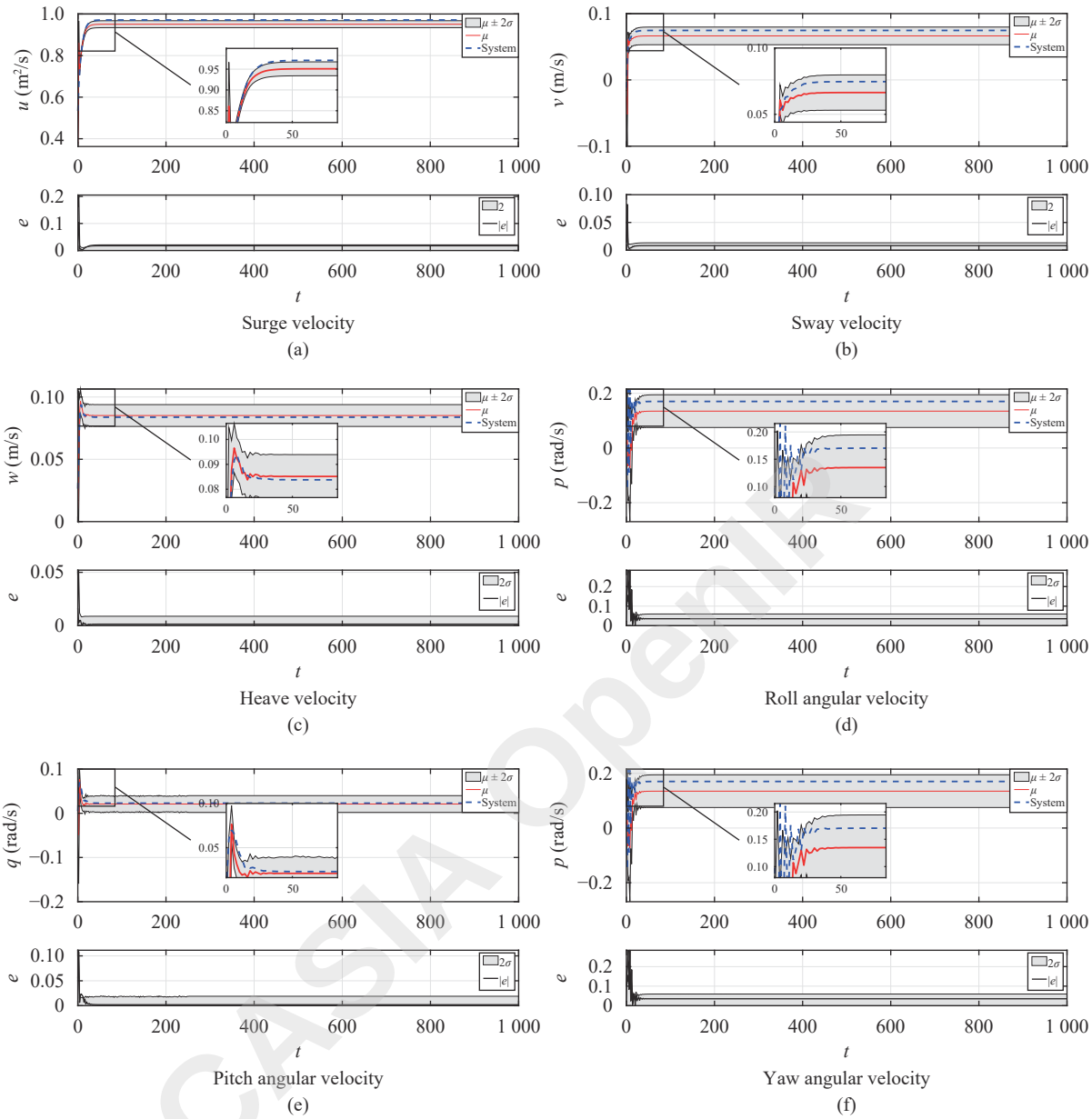

Fig. 7 Multi-output GPs validation with unknown data

learned RNN and the multi-output Gaussian processes over the total length of the simulated data. Navigation applications as EKF, UKF, and control as model predictive control require predicting the behaviour of the plant in a number of steps ahead of the actual state to predict the correct position or control signals. In the case of the multi-output GPs, the simulation is done by feeding back to the simulation the past inputs $y_i(k-n)$. The initial position and control signals of rudder, elevator and forward speed were used. The naive simulation[2] covers training and validation data acquired from the original simulation in a close loop setup. Naive simulation provides an approximation where variance is not exactly the same as previous steps, but provides a general guidance on uncertainty in the model deployment which is sufficient for our study. Suppose the variance is to be employed, such as in a control system or a navigation problem. In that case, the uncertainty propagation can be included with the use a simulation-based on Monte Carlo numerical approximation[2]. Fig. 8 shows the results from the simulation of RNN 1, RNN 2, and the multi-output GPs compared to the original system. RNN 1 compared to RNN 2 shows better performance with ramp input signals, and RNN 2 shows better performance to simulate step functions in our simulations. However, multi-output GPs can identify the system correctly and predict the behaviour of the system with chirp+ramp and chirp+step functions. The better capability of GPs to predict outside the training horizon from a number of different variations from the initial training data is confirmed by the results of Tables 3–5. The mean value of the output root-mean-square error (RMSE), the predicted residual error

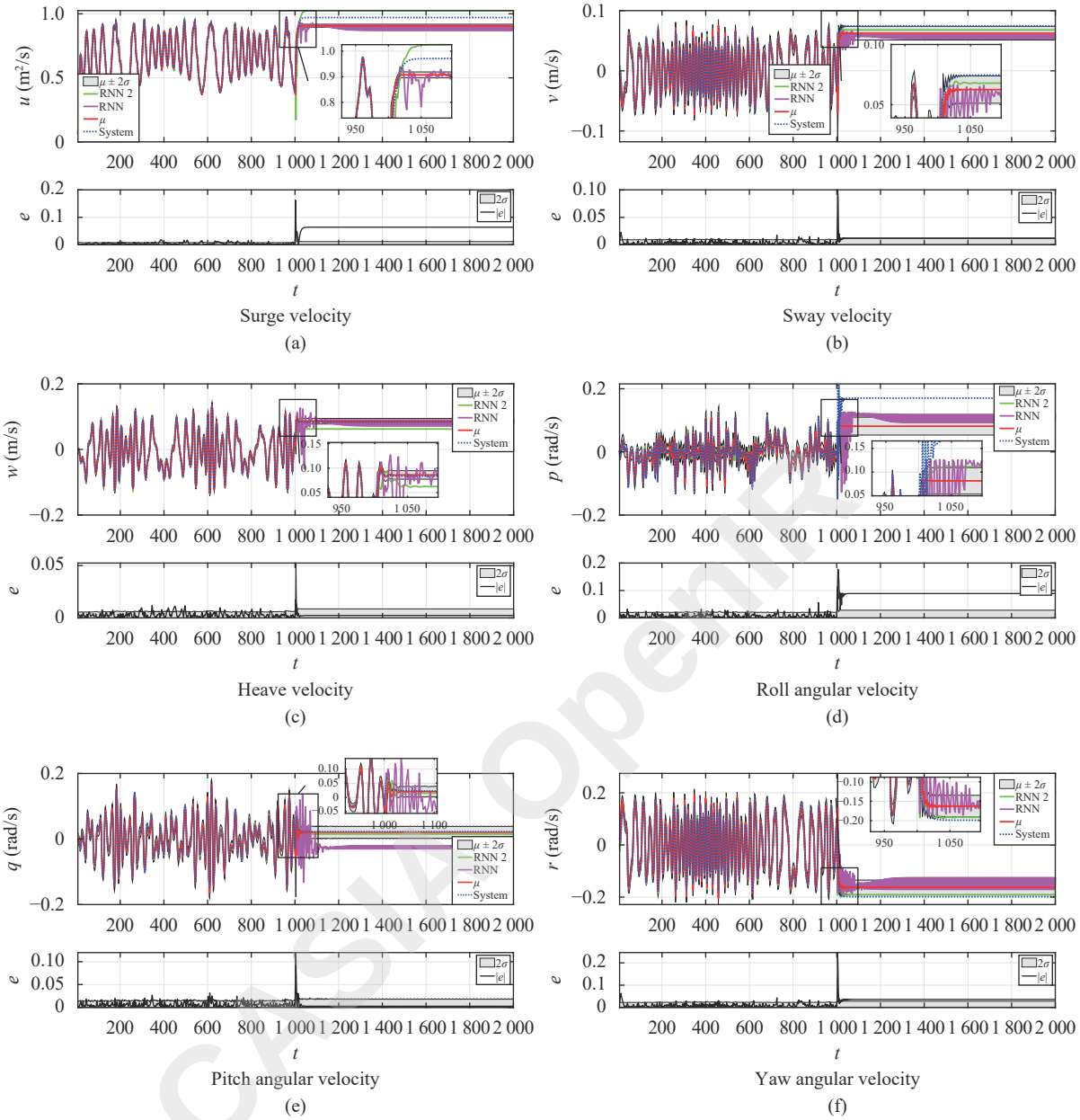

Fig. 8 Multi-output GPs simulation compared with RNN 1, RNN 2 and real system with chirp+ramp in all inputs

sum of squares (PRESS), and mean absolute error (MAE) for GPs are smaller than the values of RNN 1 and RNN 2.

A secondary set of simulations were also carried out to research the sensibility of multi-output GPs compared to both RNNs in respect to the increase in training data. A series of simulations at 500, 1 000, 1 500, 2 000, and 4 000 seconds were carried out with commands signals composed of a chirp signal for half of the time and a ramp signal for the other half of the simulation. The first half of each data set was employed for training, and the test simulation of the learned model was done over the complete extension of data. The RMSE, PRESS, and MAE were also measured for all the simulation results. The result of the sensitivity analysis can be seen in Figs. 9 and 10. All the measurements of the sensitivity analysis show the same trend for each measured variable. The simulations with 1 500 seconds of capture data for RNN 1 and GPs show similar average results, and RNN 1 over 4 000 seconds of simulation can overpass the ability of GPs to simulate the system with a chirp+ramp signal for all inputs. RNN 2 and RNN 1 require a higher quantity of data of rich data to be effective in the simulation of AUV outside of the learning horizon compared to multi-output GPs.

5 Conclusions

In this work, the use of multi-output GPs for the system identification of AUV dynamics was tested on a Remus 100 AUV. It was demonstrated that the non-parametric

Table 3 RMSE results for all simulations, average and standard deviation

Simulation number	GP	RNN 1	RNN 2
1	1.85E-02	5.27E-02	6.34E-02
2	1.48E-02	1.76E-02	6.96E-02
3	1.69E-02	1.34E-02	3.83E-02
4	2.31E-02	5.12E-02	5.12E-02
5	2.88E-02	3.59E-02	4.07E-02
6	1.18E-02	1.68E-02	2.60E-02
7	1.46E-02	3.09E-02	2.70E-02
8	2.64E-02	2.02E-02	3.45E-02
Average	1.94E-02	2.98E-02	4.38E-02
Standard deviation	3.71E-05	2.43E-04	2.61E-04

Table 4 MAE results for all simulations, average and standard deviation

Simulation number	GP	RNN 1	RNN 2
1	1.19E-02	2.04E-02	3.51E-02
2	9.51E-03	1.00E-02	4.02E-02
3	1.20E-02	8.87E-03	2.07E-02
4	1.59E-02	3.32E-02	3.03E-02
5	1.78E-02	2.08E-02	2.36E-02
6	8.43E-03	9.67E-03	1.48E-02
7	9.92E-03	1.82E-02	1.45E-02
8	2.21E-02	3.19E-01	1.60E-02
Average	1.35E-02	5.50E-02	2.44E-02
Standard deviation	2.27E-05	1.14E-02	9.58E-05

Table 5 PRESS results for all simulations, average and standard deviation

Simulation number	GP	RNN 1	RNN 2
1	4.69E-01	7.89E+00	4.33E+00
2	2.61E-01	5.41E-01	9.96E+00
3	4.54E-01	2.14E-01	1.68E+00
4	9.58E-01	4.15E+00	2.91E+00
5	1.10E+00	2.03E+00	2.22E+00
6	1.54E-01	4.78E-01	8.60E-01
7	2.48E-01	2.12E+00	1.00E+00
8	1.18E+00	6.67E-01	1.50E+00
Average	6.03E-01	2.26E+00	3.06E+00
Standard deviation	1.70E-01	6.89E+00	9.05E+00

multi-output GPs can model an AUV as well as RNN with the added value of a confidence measurement. In the simulations, GPs show a better ability than RNN to predict and simulate the behaviour of an AUV. In some cases, GPs performed better than RNN outside of the

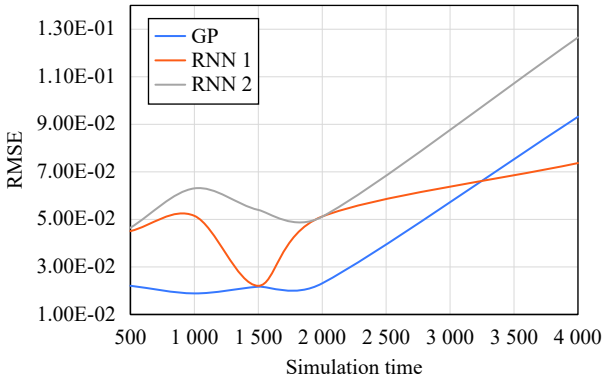

Fig. 9 RMSE results of training size sensitivity analysis

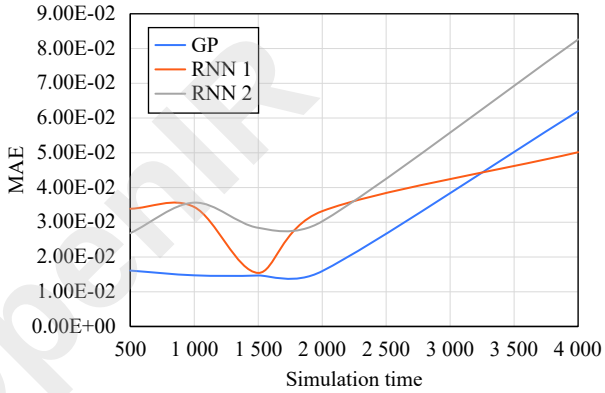

Fig. 10 MAE results of training size sensitivity analysis

training horizons, with the error between the GPs and the real system being relatively low as the convolution process is equivalent to representing the system through a differential equation. The GPs model obtained also has a smaller number of hyperparameters compared to a large number of coefficients in a mathematical model. The results of the sensitivity analysis show that multi-output GPs perform better than RNN with low quantities of data. RNN required a higher spectrum of data to be able to approximate the behaviour of the vehicle outside of the training horizon. The research demonstrated the viability and robustness of multi-output GPs in modelling AUVs. The non-parametric form and capability of modelling relation between outputs can allow new control methodologies for underwater vehicles.

To improve further the capability of prediction of the system, more recent suggested techniques for GPs such as recurrent GPs can be used. The simulation of GPs can be also improved if techniques such as Monte Carlo and Taylor series can take advantage of the variance to increase the horizon of cover maneuvers and the prediction accuracy. The subsequent work will be devoted to the development of model-based reinforced learning using the obtained model. Furthermore, the real world is a noisy environment that can be better described with Gaussian distributions that include coupling between DoFs.

References

[1] J. Rodriguez, H. Castañeda, J. L. Gordillo. Lagrange modeling and navigation based on quaternion for controlling a micro AUV under perturbations. *Robotics and Autonomous Systems*, vol. 124, Article number 103408, 2020. DOI: 10.1016/j.robot.2019.103408.

[2] J. Kocijan. *Modelling and Control of Dynamic Systems Using Gaussian Process Models*, Cham, Germany: Springer, 2016. DOI: 10.1007/978-3-319-21021-6.

[3] B. Allotta, R. Costanzi, L. Pugi, A. Ridolfi, A. Rindi. Fast calibration procedure of the dynamic model of an autonomous underwater vehicle from a reduced set of experimental data. *Advances in Italian Mechanism Science*, G. Boschetti, A. Gasparetto, Eds., Cham, Germany: Springer, pp. 317–326, 2017. DOI: 10.1007/978-3-319-48375-7_34.

[4] R. E. D. Bishop, A. G. Parkinson. On the planar motion mechanism used in ship model testing. *Philosophical Transactions of the Royal Society A: Mathematical, Physical and Engineering Sciences*, vol. 266, no. 1171, pp. 35–61, 1970. DOI: 10.1098/rsta.1970.0002.

[5] F. J. Velasco, E. R. Herrero, F. J. L. Santos, J. M. R. Rodríguez, J. J. D. Hernández, L. M. V. Antolín. Measurements of hydrodynamic parameters and control of an underwater torpedo-shaped vehicle. *IFAC-PapersOnLine*, vol. 48, no. 2, pp. 167–172, 2015. DOI: 10.1016/j.ifacol.2015.06.027.

[6] B. Allotta, R. Costanzi, L. Pugi, A. Ridolfi. Identification of the main hydrodynamic parameters of typhoon AUV from a reduced experimental dataset. *Ocean Engineering*, vol. 147, pp. 77–88, 2018. DOI: 10.1016/j.oceaneng.2017.10.032.

[7] J. Park, S. H. Rhee, H. K. Yoon, S. Lee, J. Seo. Effects of a propulsor on the maneuverability of an autonomous underwater vehicle in vertical planar motion mechanism tests. *Applied Ocean Research*, vol. 103, Article number 102340, 2020. DOI: 10.1016/j.apor.2020.102340.

[8] H. Suzuki, J. Sakaguchi, T. Inoue, Y. Watanabe, H. Yoshida. Evaluation of methods to estimate hydrodynamic force coefficients of underwater vehicle based on CFD. *IFAC Proceedings Volumes*, vol. 46, no. 33, pp. 197–202, 2013. DOI: 10.3182/20130918-4-JP-3022.00026.

[9] A. Tyagi, D. Sen. Calculation of transverse hydrodynamic coefficients using computational fluid dynamic approach. *Ocean Engineering*, vol. 33, no. 5–6, pp. 798–809, 2006. DOI: 10.1016/j.oceaneng.2005.06.004.

[10] S. A. T. Randeni P, Z. Q. Leong, D. Ranmuthugala, A. L. Forrest, J. Duffy. Numerical investigation of the hydrodynamic interaction between two underwater bodies in relative motion. *Applied Ocean Research*, vol. 51, pp. 14–24, 2015. DOI: 10.1016/j.apor.2015.02.006.

[11] B. Das, B. Subudhi, B. B. Pati. Cooperative formation control of autonomous underwater vehicles: An overview. *International Journal of Automation and Computing*, vol. 13, no. 3, pp. 199–225, 2016. DOI: 10.1007/s11633-016-1004-4.

[12] S. K. Shariati, S. H. Mousavizadegan. The effect of appendages on the hydrodynamic characteristics of an underwater vehicle near the free surface. *Applied Ocean Research*, vol. 67, pp. 31–43, 2017. DOI: 10.1016/j.apor.2017.07.001.

[13] J. D. Liu, H. S. Hu. Biologically inspired behaviour design for autonomous robotic fish. *International Journal of Automation and Computing*, vol. 3, no. 4, pp. 336–347, 2006. DOI: 10.1007/s11633-006-0336-x.

[14] D. Sen. A study on sensitivity of maneuverability performance on the hydrodynamic coefficients for submerged bodies. *Journal of Ship Research*, vol. 45, no. 3, pp. 186–196, 2000. DOI: 10.5957/jsr.2000.44.3.186.

[15] K. P. Rhee, S. Y. Lee, Y. J. Sung. Estimation of manoeuvring coefficients from PMM test by genetic algorithm. In *Proceedings of International Symposium and Workshop on Force Acting on a Manoeuvring Vessel*, Val de Reuil, France, pp. 77–87, 1998.

[16] A. Ross, T. I. Fossen, T. A. Johansen. Identification of underwater vehicle hydrodynamic coefficients using free decay tests. *IFAC Proceedings Volumes*, vol. 37, no. 10, pp. 363–368, 2004. DOI: 10.1016/S1474-6670(17)31759-7.

[17] E. Shahinfar, M. Bozorg, M. Bidoky. Parameter estimation of an AUV using the maximum likelihood method and a Kalman filter with fading memory. *IFAC Proceedings Volumes*, vol. 43, no. 16, pp. 1–6, 2010. DOI: 10.3182/20100906-3-IT-2019.00003.

[18] M. T. Sabet, P. Sarhadi, M. Zarini. Extended and unscented Kalman filters for parameter estimation of an autonomous underwater vehicle. *Ocean Engineering*, vol. 91, pp. 329–339, 2014. DOI: 10.1016/j.oceaneng.2014.09.013.

[19] H. Shariati, H. Moosavi, M. Danesh. Application of particle filter combined with extended Kalman filter in model identification of an autonomous underwater vehicle based on experimental data. *Applied Ocean Research*, vol. 82, pp. 32–40, 2019. DOI: 10.1016/j.apor.2018.10.015.

[20] T. Perez, T. I. Fossen. Practical aspects of frequency-domain identification of dynamic models of marine structures from hydrodynamic data. *Ocean Engineering*, vol. 38, no. 2–3, pp. 426–435, 2011. DOI: 10.1016/j.oceaneng.2010.11.004.

[21] P. W. J. van de Ven, T. A. Johansen, A. J. Sørensen, C. Flanagan, D. Toal. Neural network augmented identification of underwater vehicle models. *Control Engineering Practice*, vol. 15, no. 6, pp. 715–725, 2007. DOI: 10.1016/j.conengprac.2005.11.004.

[22] F. Xu, Z. J. Zou, J. C. Yin, J. Cao. Parametric identification and sensitivity analysis for autonomous underwater vehicles in diving plane. *Journal of Hydrodynamics*, vol. 24, no. 5, pp. 744–751, 2012. DOI: 10.1016/S1001-6058(11)60299-0.

[23] M. Zhang, Y. X. Xu, B. Li, D. N. Wang, W. Xu. A modular autonomous underwater vehicle for environmental sampling: System design and preliminary experimental results. In *Proceedings of OCEANS 2014 – TAIPEI*, IEEE, Taipei, China, pp. 1–5, 2014. DOI: 10.1109/OCEANS-TAIPEI.2014.6964495.

[24] P. van de Ven, C. Flanagan, D. Toal. Identification of underwater vehicle dynamics with neural networks. In *Proceedings of OCEANS'04 MTTS/IEEE Techno-Ocean*, IEEE, Kobe, Japan, pp. 1198–1204, 2004. DOI: 10.1109/OCEANS.2004.1405750.

[25] F. Xu, Z. J. Zou, J. C. Yin, J. Cao. Identification modeling of underwater vehicles' nonlinear dynamics based on support vector machines. *Ocean Engineering*, vol. 67, pp. 68–76, 2013. DOI: 10.1016/j.oceaneng.2013.02.006.

[26] V. S. Kodogiannis, P. J. G. Lisboa, J. Lucas. Neural net-

work modelling and control for underwater vehicles. *Artificial Intelligence in Engineering*, vol. 10, no. 3, pp. 203–212, 1996. DOI: 10.1016/0954-1810(95)00029-1.

[27] J. Brownlee. *Master Machine Learning Algorithms: Discover How They Work and Implement Them from Scratch*. Machine Learning Mastery, 2016.

[28] M. P. Deisenroth, C. E. Rasmussen. PILCO: A model-based and data-efficient approach to policy search. In *Proceedings of the 28th International Conference on Machine Learning*, ACM, Bellevue, USA, pp. 465−472, 2011.

[29] S. Kashmiri, S. Payandeh. Robot navigation controller: A non-parametric regression approach. *IFAC Proceedings Volumes*, vol. 43, no. 22, pp. 22–27, 2010. DOI: 10.3182/20100929-3-RO-4017.00005.

[30] D. G. Krige. A statistical approach to some basic mine valuation problems on the witwatersrand. *Journal of the Southern African Institute of Mining and Metallurgy*, vol. 52, no. 6, pp. 119–139, 1951.

[31] B. Wehbe, M. Hildebrandt, F. Kirchner. Experimental evaluation of various machine learning regression methods for model identification of autonomous underwater vehicles. In *Proceedings of IEEE International Conference on Robotics and Automation*, IEEE, Singapore, pp. 4885−4890, 2017. DOI: 10.1109/ICRA.2017.7989565.

[32] J. Kocijan, A. Grancharova. Gaussian process modelling case study with multiple outputs. *Comptes Rendus de l'Académie Bulgare des Sciences*, vol. 63, no. 4, pp. 601–607, 2010.

[33] W. Ariza Ramirez, Z. Q. Leong, H. D. Nguyen, S. G. Jayasinghe. Exploration of the applicability of probabilistic inference for learning control in underactuated autonomous underwater vehicles. *Autonomous Robots*, vol. 44, no. 6, pp. 1121–1134, 2020. DOI: 10.1007/s10514-020-09922-z.

[34] M. A. Álvarez, N. D. Lawrence. Computationally efficient convolved multiple output Gaussian processes. *Journal of Machine Learning Research*, vol. 12, pp. 1459–1500, 2011.

[35] J. Zhao, S. L. Sun. Variational dependent multi-output Gaussian process dynamical systems. *Journal of Machine Learning Research*, vol. 17, pp. 1–36, 2016.

[36] M. A. Álvarez, N. D. Lawrence. Sparse convolved Gaussian processes for multi-output regression. In *Proceedings of the 21st International Conference on Neural Information Processing Systems*, Vancouver, Canada, pp. 57−64, 2009.

[37] W. Ariza Ramirez, Z. Q. Leong, H. Nguyen, S. G. Jayasinghe. Non-parametric dynamic system identification of ships using multi-output Gaussian processes. *Ocean Engineering*, vol. 166, pp. 26–36, 2018. DOI: 10.1016/j.oceaneng.2018.07.056.

[38] T. I. Fossen. *Guidance and Control of Ocean Vehicles*, New York, USA: Wiley, 1994.

[39] M. Gertler, G. R. Hagen. Standard Equations of Motion for Submarine Simulation, Technical Report 2510, David W Taylor Naval Ship Research and Development Center, Bethesda, USA, 1967.

[40] T. Prestero. Verification of A Six-degree of Freedom Simulation Model for the Remus Autonomous Underwater Vehicle, Master dissertation, Massachusetts Institute of Technology, USA, 2001.

[41] J. Kim, W. K. Chung. Accurate and practical thruster modeling for underwater vehicles. *Ocean Engineering*, vol. 33, no. 5−6, pp. 566–586, 2006. DOI: 10.1016/j.oceaneng.2005.07.008.

[42] M. Ebden. Gaussian Processes for Regression: A Quick Introduction, The Website of Robotics Research Group in Department on Engineering Science, University of Oxford, UK, 2008.

[43] D. Higdon. Space and space-time modeling using process convolutions. *Quantitative Methods for Current Environmental Issues*, C. W. Anderson, V. Barnett, P. C. Chatwin, A. H. El-Shaarawi, Eds., London, UK: Springer, pp. 37−56, 2002. DOI: 10.1007/978-1-4471-0657-9_2.

[44] P. Boyle, M. R. Frean. Dependent Gaussian processes. In *Proceedings of the 17th International Conference on Neural Information Processing Systems*, Vancouver, Canada, pp. 217−224, 2004.

[45] M. Alvarez, N. Lawrence. Multiple output Gaussian processes in Matlab. 2014.

[46] C. A. Micchelli, Y. S. Xu, H. Z. Zhang. Universal kernels. *The Journal of Machine Learning Research*, vol. 7, pp. 2651–2667, 2006.

[47] C. E. Rasmussen, C. K. I. Williams. *Gaussian Processes for Machine Learning*, Massachusetts, USA: The MIT Press, 2006.

[48] R. Hall, S. Anstee. Trim Calculation Methods for A Dynamical Model of the Remus 100 Autonomous Underwater Vehicle, Technical Report DSTO-TR-2576, Defence Science and Technology Organisation, Edinburgh, Australia, 2011.

Wilmer Ariza Ramirez received the B. Sc. degree in mechatronic engineering from Universidad San Buenaventura, Colombia in 2009, and the M. Eng. degree in advances manufacturing technology from Swinburne University of Technology, Australia in 2013. He is currently a Ph.D. degree candidate in maritime engineering at Australian maritime College, University of Tasmania, Australia.

His research interests include simultaneous localization and mapping, navigation, path planning, intelligent systems, and nonlinear control with the use of machine learning algorithms for underwater vehicles.

E-mail: wilmer.arizaramirez@utas.edu.au

ORCID iD: 0000-0002-2755-2281 (Corresponding author)

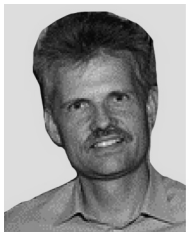

Juš Kocijan received the Ph. D. degree in electrical engineering from Faculty of Electrical Engineering, University of Ljubljana, Slovenia in 1993. He is currently a senior researcher with the Jožef Stefan Institute, Slovenia, and a professor of electrical engineering with University of Nova Gorica, Slovenia. His other activities include serving as editor and on the editorial boards of research journals, serving as a member of the IFAC technical committee on computational intelligence in control. He is a senior member of the IEEE Control Systems Society, and a member of SLOSIM − Slovenian Society for Simulation and Modelling and Automatic Control Society of Slovenia.

His research interests include modeling and control of dynamic systems.

E-mail: jus.kocijan@ijs.si

Zhi Quan Leong received the B. Eng. degree in ocean engineering and the Ph. D. degree in maritime engineering from Australian Maritime College, University of Tasmania, Australia in 2015. He is currently a research fellow (DSTG) at Australian Maritime College, and a lecture of hydrodynamics, computational fluid dynamics at University of Tasmania, Australia. He is currently involved in an international research team led by Australia′s Defence Science and Technology Group to refine the methods that will be used to test the hydrodynamic performance of underwater vehicles.

His research interests include ship and platform hydrodynamics, naval architecture, marine engineering, ocean engineering, special vehicles, maritime engineering, navigation and position fixing.

E-mail: Zhi.Leong@utas.edu.au

Hung Duc Nguyen received the B. Eng. degree in ship navigation engineering from Vietnam Maritime University, Vietnam in 1991, and the M. Eng. and Ph. D. degrees in marine systems engineering from Tokyo University of Marine Science and Technology, Japan in 2001. He is currently a lecturer of marine control engineering with National Centre for Maritime Engineering and Hydrodynamics, Australian Maritime College, University of Tasmania, Australia.

His research interests include guidance, navigation and control of marine vehicles and offshore structures, ship maneuvering dynamics and manoeuvrability, global positioning system (GPS), global navigation satellite system (GNSS) and inertial navigation systems, linear and non-linear control systems, modeling and recursive/stochastic estimation of marine and offshore control systems, fault detection and monitoring based on modeling and estimation, instrumentation and process control, seakeeping and roll stabilization systems, and marine robots and control applications in marine vehicles including underwater vehicles.

E-mail: h.d.nguyen@utas.edu.au

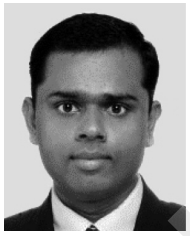

Shantha Gamini Jayasinghe received the B. Sc. degree in electronics and telecommunication engineering from University of Moratuwa, Sri Lanka in 2003, and the Ph.D. degree in electrical engineering from Nanyang Technological University, Singapore in 2013. From 2011 to 2015, he worked as an electrical systems engineer at Rolls Royce Advanced Technology Centre in Singapore. He is currently a lecturer of maritime electrical engineering at Australian Maritime Collage, University of Tasmania, Australia. He has authored or co-authored over 70 international journal and conference papers and three book chapters. He holds seven US/UK patents.

His research interests include power electronic converters, renewable energy technologies, grid integration of energy systems, shipboard power systems, electric propulsion and control systems.

E-mail: shantha.jayasinghe@utas.edu.au